Magnonic Einstein–de Haas Effect: Ultrafast Rotation of Magnonic Microspheres

A. Kani,[*] F. Quijandría, and J. Twamley

Quantum Machines Unit, Okinawa Institute of Science and Technology Graduate University, Okinawa 904-0495, Japan

Magnons, collective spin excitations in magnetic crystals, have attracted much interest due to their ability to couple strongly to microwaves and other quantum systems. In compact magnetic crystals, we show that there are magnonic modes that can support orbital angular momentum and that these modes can be driven by linearly polarized microwave fields. Because of conservation of angular momentum, exciting such magnon modes induces a mechanical torque on the crystal. We study a levitated magnetic crystal, a yttrium iron garnet (YIG) microsphere, where such orbital angular momentum magnon modes are driven by microwaves held in a microwave high-Q microwave cavity. We find that the YIG sphere experiences a mechanical torque and can be spun up to ultralarge angular speeds exceeding 10 GHz.

Over a century ago, two related effects were experimentally demonstrated. The first one is the Einstein–de Haas (EdH) effect in which the alignment of initially random magnetic moments by a magnetizing field causes the object to rotate [1–4]. The second one is the Barnett effect where the rotation of an object containing magnetic moments causes them to align or magnetize [5–7]. Both are a consequence of the conservation of the angular momentum. These gyromagnetic effects enable the experimental probing of how angular momenta and magnetic moments are related, and played an important role in understanding the origin of the latter. Magnetic moments within magnetic crystals are usually not isolated. Because of their mutual interactions they exhibit a collective dynamics known as spin waves (magnons) [8]. This collective spin state can support orbital angular momentum (OAM) similar to all other waves [9–13], and in principle the magnetic substance not only carries intrinsic spin angular momentum (SAM) but also OAM [14]. While the typical EdH effect relies only on the creation of polarized SAM, the excitation of OAM modes can also result in a mechanical rotation. In an unconfined geometry the existence of straightforward OAM-magnon modes is problematic [15–17]. However, in a finite dimensional crystal, spin waves are confined and also discretized [18]; thus one can resonantly excite a particular OAM mode by an ordinary microwave field to stimulate the rotation of an object. Thus, intuitively, by using a sufficiently intense microwave field one can spin up the particle to very high frequencies.

In this Letter, we explore the magnonic OAMs naturally supported by spherical ferromagnetic crystals and their related gyromagnetic effects. Spherical ferromagnetic crystals support plenty of magnon modes [18,19]. The simplest of those is the uniformly precessing Kittel mode which has been extensively studied [20–22]. However, the OAM is embedded in the spatial distribution of the magnetization of higher order magnon modes [23]. We propose a microwave cavity setup where we exploit the spatial distribution of the standing waves of the electromagnetic field to couple and excite the OAM modes within the spherical magnet. Magnons can strongly couple to the cavity field [24] and exert a giant mechanical torque. Unlike the standard EdH effect, in the magnonic version the Barnett effect hinders the mechanical rotation. We show that it is possible to compensate for the influence of the Barnett effect and obtain ultrahigh rotational speeds above 10 GHz for micron-sized particles at moderate vacuum pressures. Such ultrafast rotation can be used to explore rotational vacuum friction [25]. There are a variety of techniques for rotating a levitated particle either by using optical fields [26–29], acoustic waves [30], rotating electric fields [31], or rotating magnetic fields [32]. Record high rotational speeds of a few GHz have been achieved by transferring optical angular momentum to nanoparticles [27,29,33]. We note that the EdH effect does not involve the transfer of angular momentum from an external source. Through the mechanical rotation we can manipulate the magnetic properties of the material due to the intertwined Barnett effect [34]. The recent developments of hybrid quantum systems involving magnon modes could also exploit OAM properties of these modes for a variety of purposes including the control of mechanical rotation [35–37].

Background on OAM-magnon modes.—We consider a small spherical isotropic ferromagnetic insulator that is fully magnetized along e_z by applying a large static

homogeneous magnetic field ($H_0 = H_0 e_z$). Each magnetic moment (μ) carries a SAM of $S = -\mu/\gamma$ [38], where γ is the gyromagnetic ratio. If the moments do not interact with each other, an arbitrary moment deviating from the ordered state experiences a torque $dS/dt = -(d\mu/dt)/\gamma = \mu_0\mu \times H_0$ and precesses independently about the bias magnetic field at the Larmor frequency $\omega = \gamma\mu_0 H_0$ [39]. However, the magnetic moments are coupled to each other through the magnetic field generated by other moments, and as a result all the moments precess collectively. The collective magnetization precession, or the spin wave, is described by solving the Landau-Lifshitz equation $dM(r, t)/dt = -\gamma\mu_0 M \times H$ along with Maxwell's equations with appropriate boundary conditions. Here, $H = H_0 + H_i(M)$ includes the field generated by the collective moments (H_i). Although the Landau-Lifshitz equation is nonlinear the spin waves are typically assumed as a small deviation from the macroscopic magnetization, $M = M_s e_z + m(r, t)$, where M_s is the saturation magnetization of the ferromagnet and $m(r, t)$ is the spin wave magnetization. There are an infinite number of magnon modes in a spherical crystal [18,40], and each mode is described using three indices (n, m, q) with $n \in \mathbb{N}$, $m = -n, ..., n$, and $q = 0, 1, ..., q_{\max}(n, m)$ [19]. The eigenfrequencies and the associated magnetization distribution for the first few magnon modes of a sphere are shown in Fig. 1. The phase structure associated with the magnon modes can be related to the OAM. A general magnon mode has a complex magnetization profile [18,40,41]. Most of them are hybrid OAM modes except the families $(n, m = n)$ and $(n, m = n - 1)$ which are pure OAM eigenmodes [23]. For these

two families $q_{\max} = 0$; hence we drop the third index q. The magnetization vector of these OAM eigenmodes [19] in the Schrödinger picture can be written as

$$\hat{m}_{n,m} = M_0 \frac{\rho^{m-1} z^{n-m}}{R^{n-1}} (e_x + ie_y)e^{-i(1-m)\phi}\hat{s} + \text{H.c.}, \quad (1)$$

where $M_0 = \sqrt{[2^{n-m+1}\gamma\hbar M_s\Gamma(n + \frac{3}{2})]/[3V\sqrt{\pi}\Gamma(m)]}$ is the zero-point magnetization [40], $\hat{s}$ is the bosonic annihilation operator for the magnon mode (n, m), R is the radius of the sphere, V is the volume of the sphere, (ρ, ϕ, z) are cylindrical coordinates, and (e_x, e_y, e_z) are the Cartesian unit vectors. The time dependence of $\hat{m}_{n,m}$ is determined by the self Hamiltonian $\hat{H}_{\hat{s}^\dagger\hat{s}} = \hbar\omega_{n,m}\hat{s}^\dagger\hat{s}$, where $\omega_{n,m} = \gamma\mu_0 H_0 + [\gamma\mu_0 M_s(3m - 2n - 1)/3(2n + 1)]$ is the resonance precessional frequencies of the OAM eigenmode. These modes carry definite OAM of $l\hbar = (1 - m)\hbar$ which is encoded on the chiral phase structure of the magnetization field $e^{-i(1-m)\phi}$ [23].

Exciting OAM-magnon modes.—Discrete magnon modes can be addressed by a resonant microwave field. One does not require a field carrying OAM to couple and drive a magnonic OAM mode. However, it is necessary to have some spatial mode matching of the microwave magnetic field with the magnonic mode. In principle one can carefully engineer the microwave magnetic field to couple to any specific magnonic OAM mode [42,43]. In this Letter, we consider a linearly polarized microwave cavity mode whose magnetic component is of the form $\hat{B} = ie_y B_0 \sin(kx + \delta)(\hat{a}^\dagger - \hat{a})$, where $\hat{a}$ is the bosonic
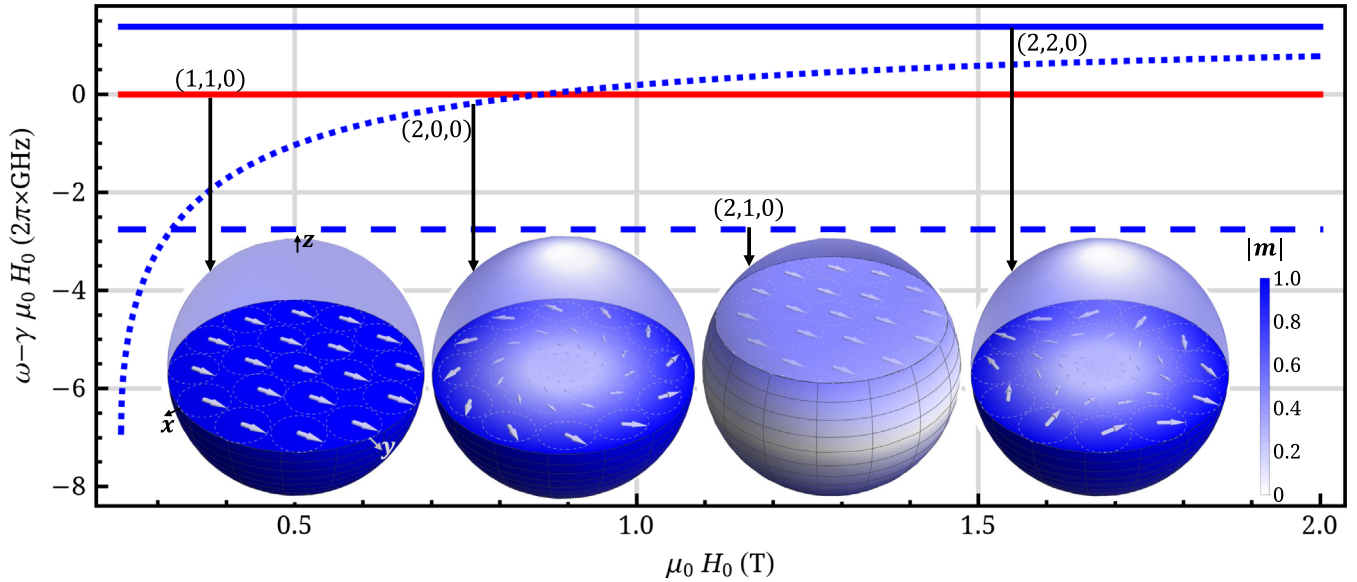

FIG. 1. Magnon modes in a ferromagnetic sphere. Eigenfrequencies of the first few magnon modes as a function of the bias magnetic field H_0. All the eigenfrequencies are offset by $\gamma\mu_0 H_0$, the Kittel mode frequency. The choice of parameters $M_s = 5.87 \times 10^5$ Am^{-1} and $\gamma = 2\pi \times 28$ GHz corresponds to YIG [40]. The inset figures show the precessing magnetization distribution $m(x, y, z)$ of these magnon modes.

annihilation operator for the microwave cavity mode, B_0 is the zero-point magnetic field, k is the microwave field wave number, and δ is the phase at the position of the spherical magnetic particle. The cavity-magnon coupling can be very well described by the magnetic dipole interaction

$$\hat{H}_{\text{int}} = -\int \hat{\boldsymbol{m}} \cdot \hat{\boldsymbol{B}} dV. \tag{2}$$

For a sphere size much smaller than the cavity field wavelength ($\sim$cm), the cavity magnetic field can be approximated as $\hat{\boldsymbol{B}} \approx i\boldsymbol{e}_y B_0 (\sin\delta + kx\cos\delta)(\hat{\boldsymbol{a}}^\dagger - \hat{\boldsymbol{a}})$, up to first order in x. The overlap between the cavity and the magnon modes [Eq. (2)] can be estimated to find the selection rules. In a linearly inhomogeneous magnetic field, $\hat{H}_{\text{int}} \neq 0$ only for the Kittel mode and the lowest OAM modes (2,0) and (2,2). Here, we focus on exciting the (2,2) magnon mode which is a pure OAM eigenmode. As seen from Fig. 1, the resonance frequency of the (2,2) magnon mode is substantially different from that of the (1,1) and (2,0) modes. Thus, we can resonantly couple the cavity only to the (2,2) mode. The coupling can be maximized by trapping the sphere at a node of the cavity magnetic field where the spatial mode overlap is maximum. Under the rotating wave approximation, the interaction between the cavity and the (2,2) OAM-magnon mode [Eq. (2)] takes the form

$$\hat{H}_{\text{int}} = \frac{4\pi}{15} kR^4 M_0 B_0 (\hat{\boldsymbol{a}}\hat{s}^\dagger + \hat{\boldsymbol{a}}^\dagger \hat{s}) \equiv \hbar g(\hat{\boldsymbol{a}}\hat{s}^\dagger + \hat{\boldsymbol{a}}^\dagger \hat{s}), \tag{3}$$

where g denotes the cavity-magnon coupling strength.

OAM conversion.—We observe that although Eq. (3) describes the interaction between a linearly polarized microwave cavity field (which does not carry any angular momentum) and an OAM-magnon mode, the total angular momentum must be conserved as the OAM-magnon mode is being excited. In order to show this, we now compute the mechanical force and torque acting on the particle. The force density acting on a magnetic crystal in an electromagnetic field is given by [44,45]

$$\hat{\boldsymbol{f}} = (\hat{\boldsymbol{m}} \cdot \nabla)\hat{\boldsymbol{B}} - \frac{1}{c^2}\frac{d\hat{\boldsymbol{m}}}{dt} \times \hat{\boldsymbol{E}}, \tag{4}$$

where $\hat{\boldsymbol{E}} \approx \boldsymbol{e}_z cB_0 (\hat{\boldsymbol{a}}^\dagger + \hat{\boldsymbol{a}})$ is the cavity electric field at the position of the particle and c is the velocity of light. Integrating Eq. (4), $\hat{\boldsymbol{F}} = \int \hat{\boldsymbol{f}} dV$, gives the net force acting on the center of mass. In the linear inhomogeneous magnetic field, only the excitation of the Kittel mode generates force and excites center-of-mass motion [40]. Since instead we target the (2,2) OAM-magnon mode, the center-of-mass motion is decoupled. The net mechanical torque acting about the center of mass can be written as

$$\hat{\boldsymbol{\tau}} = \int \hat{\boldsymbol{r}} \times \hat{\boldsymbol{f}} dV = i\hbar g(\hat{\boldsymbol{a}}^\dagger \hat{s} - \hat{\boldsymbol{a}}\hat{s}^\dagger)\boldsymbol{e}_z. \tag{5}$$

This nonzero torque tends to rotate the particle about the z axis. From the interaction Hamiltonian [Eq. (3)], the rate of excitation of the magnon mode $d(\hat{s}^\dagger \hat{s})/dt = i[\hat{H}_{\text{int}}, \hat{s}^\dagger \hat{s}]/\hbar$ can be written as

$$\frac{d}{dt}\hat{s}^\dagger \hat{s} = ig(\hat{\boldsymbol{a}}^\dagger \hat{s} - \hat{\boldsymbol{a}}\hat{s}^\dagger). \tag{6}$$

Comparing Eqs. (5) and (6), we can write the rate of change of mechanical angular momentum $\hat{\boldsymbol{J}}$ of the particle as

$$\hat{\boldsymbol{\tau}} = \frac{d\hat{\boldsymbol{J}}}{dt} = -\frac{d}{dt}(l\hbar\hat{s}^\dagger \hat{s}), \tag{7}$$

and conclude that the particle acquires opposite mechanical angular momentum at the same rate at which the OAM of the magnon mode is being excited, thus guaranteeing the conservation of the total angular momentum. Note that $l = -1$ for the mode under consideration, and $l\hbar\hat{s}^\dagger \hat{s}$ is the total OAM of the excited magnon.

Results and discussion.—Now, we examine the rotational dynamics of a YIG sphere levitated inside a driven Fabry-Pérot microwave cavity [46] at a node of the cavity magnetic field [22]. In a cm long Fabry-Pérot cavity the directions orthogonal to the resonator axis can be open and thus accessed for trapping and probing the microsphere. YIG can have magnetocrystalline anisotropy which could lead to unwanted couplings of the spin to rotational degree of freedom [47–49]. Such effects can be suppressed if we choose the anisotropic axis to be pointed along the z axis. In this case the magnon modes are exactly the same as in an isotropic crystal but there will be a small shift in the resonance frequency [50,51]. We treat the rigid-body rotation classically whereas the cavity-magnon coupling is treated quantum mechanically. The total Hamiltonian of the driven cavity-magnonic system in the frame rotating with the microwave drive frequency ω_l is

$$\begin{aligned} \hat{H}/\hbar = {} & \Delta_a \hat{\boldsymbol{a}}^\dagger \hat{\boldsymbol{a}} + (\Delta_s - \omega_R)\hat{s}^\dagger \hat{s} \\ & + g(\hat{\boldsymbol{a}}\hat{s}^\dagger + \hat{\boldsymbol{a}}^\dagger \hat{s}) + \Omega(\hat{\boldsymbol{a}} + \hat{\boldsymbol{a}}^\dagger), \end{aligned} \tag{8}$$

where $\Omega = \sqrt{P\gamma_a/\hbar\omega_a}$ is the amplitude of the driving field with microwave power P, ω_a is the cavity resonance frequency, γ_a is the cavity damping rate, $\Delta_a = \omega_l - \omega_a$, $\Delta_s = \omega_l - \omega_s$, and ω_R is the angular velocity of the sphere about its center of mass. We note that, if the crystal rotates about the z axis at ω_R, then the precessional frequency changes to $\omega_s + \omega_R$ as seen in the lab frame. In other words, a rotating magnetic substance generates a magnetic field $\boldsymbol{e}_z \omega_R/\mu_0 \gamma$ known as Barnett field [38,52–54]. This Barnett field shifts the magnon frequency by ω_R, and this has been taken into account in Eq. (8).

From Eqs. (8) and (5), the mean dynamics of the system is then described by

$$\dot{a} = -a\left(\frac{\gamma_a}{2} - i\Delta_a\right) - igs - i\Omega,$$

$$\dot{s} = -s\left(\frac{\gamma_s}{2} - i(\Delta_s - \omega_R)\right) - iga,$$

$$I\dot{\omega}_R = -I\gamma_R\omega_R + i\hbar g(a^*s - as^*), \qquad (9)$$

where $a = \langle\hat{a}\rangle$, $s = \langle\hat{s}\rangle$, $I = 2\mathcal{M}R^2/5$ is the moment of inertia of the sphere, γ_a and γ_s are the cavity and the magnon damping rates, respectively, and $\gamma_R = pR^2/(\eta\mathcal{M}v)$ [27,29] is the rotational drag coefficient arising from the surrounding gas friction. Here, p is the air pressure, v is the mean molecular velocity, $\mathcal{M}$ is the mass of the sphere, and η is the efficiency of angular momentum transfer between the particle and the surrounding gas molecules. YIG supports high quality magnon modes [41,51,55] with $\gamma_s/2\pi \sim$ MHz [24]. The superconducting microwave technology offers ultrahigh Q microwave cavities with $Q_{MW} > 10^{10}$ [46,56].

The numerical solution of the system of Eq. (9) is shown in Fig. 2 for a particle size $R = 1$ μm at moderate vacuum pressure $p = 10^{-4}$ mbar. Initially, the mechanical torque as well as the rotational speed increase nonlinearly due to building up of the coherence between the cavity and the magnon. In a high-Q microwave cavity, $\gamma_a/2\pi = 3$ Hz [46], the cavity-magnon system reaches the steady state in less than a few seconds. On longer timescales, taking the quasistatic approximation ($\dot{a} = \dot{s} = 0$), the mean cavity-magnomechanical torque exerted on the particle can be written as

$$\langle\tau\rangle = \frac{\hbar\gamma_s g^2\Omega^2}{|g^2 + (\frac{\gamma_a}{2} + i\Delta_a)[\frac{\gamma_s}{2} + i(\Delta_s - \omega_R)]|^2}, \qquad (10)$$
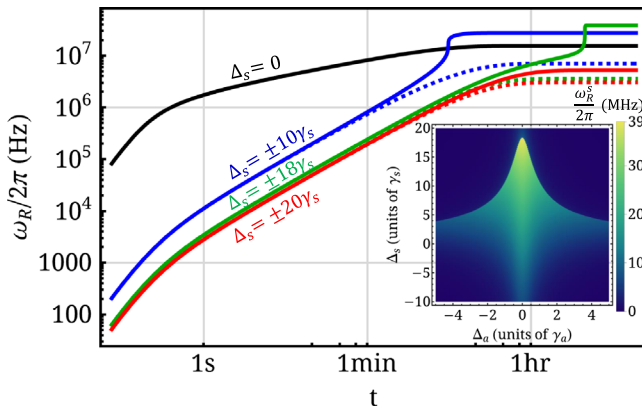

FIG. 2. Rotational frequency. Time evolution of rotational speed for different initial magnon detunings for the initial conditions $a(t = 0) = s(t = 0) = \omega_R(t = 0) = 0$. Solid and dashed lines are for positive and negative magnon detuning, respectively. Other parameters are $R = 1$ μm, $P = 10$ μW, $(\gamma_a, \gamma_s)/2\pi = (3$ Hz, 1.6 MHz$)$, $\Delta_a = 0$, and $p = 10^{-4}$ mbar. The inset shows the steady state rotational frequency as a function of the cavity and magnon detunings.

and the rotational dynamics of the particle can be described by $\dot{\omega}_R = -\gamma_R\omega_R + \langle\tau\rangle/I$. The cavity-magnon response and the resulting mechanical torque depend on $(\Delta_s - \omega_R)$, and the dynamics is nonlinear. Beyond certain detunings the rotation is bistable. If we start the particle from rest [$\omega_R(t = 0) = 0$], the system reaches to the lowest possible frequency solution, and is shown in Fig. 2. Only within the timescale where the Barnett shift is relatively small ($\omega_R(t) \ll \gamma_s$), the time evolution is linear and symmetric in Δ_s. For positive magnon detunings, at a particular time when the rotational shift compensates for the magnon detuning [$\Delta_s - \omega_R(t) = 0$] one can see a sharp rise in the rotational speed with an angular acceleration of $\langle\tau\rangle/I \sim 3.3 \times 10^7$ rad s^{-2}. However it is difficult to reach very high rotational speeds as the magnon frequency gets detuned further due to the Barnett effect. We can compensate for this rotational detuning by lowering the bias magnetic field, at the same time to achieve a very high rotational frequency.

We now examine the cases when the Barnett field is compensated, $H_0(t) = H_0(t = 0) - \omega_R(t)/\mu_0\gamma$, and optimize the coupling to produce the maximum torque and rotational speeds. In this case the mean mechanical torque is given by

$$\langle\tau\rangle = \frac{\hbar\gamma_s g^2\Omega^2}{|g^2 + (\frac{\gamma_a}{2} + i\Delta_a)(\frac{\gamma_s}{2} + i\Delta_s)|^2}. \qquad (11)$$

The rotational dynamics is linear, and the time evolution of the rotational frequency follows $\omega_R(t) = \omega_R^s[1 - \exp(-\gamma_R t)]$. The steady state rotational frequency is $\omega_R^s = \langle\tau\rangle/I\gamma_R$. The mean angular acceleration $\langle\tau\rangle/I$ of the particle is shown in Fig. 3. For a small sphere, the cavity-magnon coupling is typically weak, i.e., $g \leq \sqrt{\gamma_a\gamma_s/4}$, and the maximum torque will be exerted when both the cavity and magnon are on resonance with the microwave drive $\Delta_a = \Delta_s = 0$ [see Fig. 3(a)]. This maximum torque is

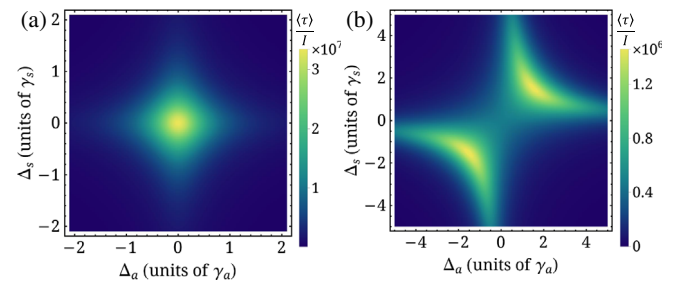$$\langle\tau\rangle_{max} = \frac{\hbar\gamma_s g^2\Omega^2}{(\frac{\gamma_a\gamma_s}{4} + g^2)^2}. \qquad (12)$$

FIG. 3. Angular acceleration. Angular acceleration $\langle\tau\rangle/I$(rad/s^2) as a function of the cavity and magnon detunings for a 1 μm (a) and a 7 μm (b) radius YIG sphere. Other parameters are the same as in Fig. 2.
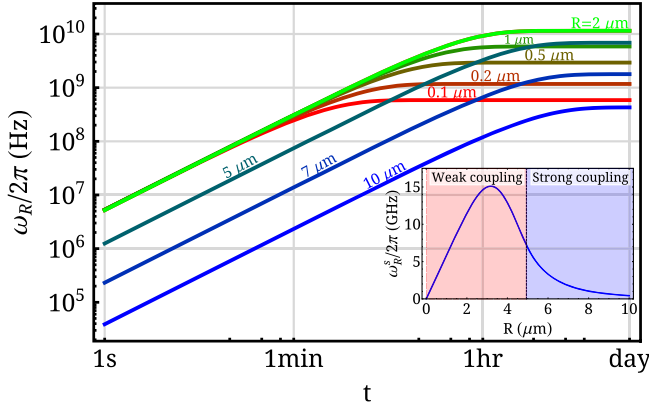
FIG. 4. Rotational dynamics when the Barnett field is compensated. Rotational dynamics for different sphere sizes at the optimal detunings. Inset: optimal steady state rotational frequency as a function of the particle size. Other parameters are the same as in Fig. 2.

Note that when $g \ll \sqrt{\gamma_a \gamma_s/4}$, irrespective of its size, the YIG sphere can be driven at a maximum angular acceleration of $\langle\tau\rangle_{\max}/I = (16\hbar g^2\Omega^2)/(I\gamma_a^2\gamma_s)$, to the angular velocity of $\langle\tau\rangle_{\max}/I\gamma_R$ in the timescale of $1/\gamma_R$. At constant pressure, as γ_R is inversely proportional to the particle size, ω_R^s increases linearly with it as shown in Fig. 4. Increasing damping rates of small particles can be compensated by lowering the pressure to obtain higher rotational speeds. For a large particle the cavity-magnon coupling is strong ($g \geq \sqrt{\gamma_a\gamma_s/4}$), which splits the resonance frequency [cf. Fig. 3(b)], and maximum torque $\langle\tau\rangle_{\max} = \hbar\Omega^2/\gamma_a$ is exerted when

$$\Delta_a = \pm\frac{\sqrt{4g^2 - \gamma_a\gamma_s}}{\sqrt{\gamma_a\gamma_s}}\frac{\gamma_a}{2}, \quad \Delta_s = \pm\frac{\sqrt{4g^2 - \gamma_a\gamma_s}}{\sqrt{\gamma_a\gamma_s}}\frac{\gamma_s}{2}. \quad (13)$$

The driving torque is constant regardless of the sphere radius and depends only on the input drive power. The steady state optimal rotational frequency ($\propto R^{-4}$) gradually decreases with the particle size. Figure 4 shows the rotational dynamics of the sphere at the optimal detuning points. We note that when the Barnett field is compensated the maximum rotational speed is 3 orders of magnitude larger. In Fig. 4 we also show the optimal steady state rotational speed as a function of the sphere size at a constant pressure $p = 10^{-4}$ mbar. Maximum rotational speed is achieved when the cavity-magnon coupling is nearly strong. For the parameters considered here, a microsphere of radius $R = 3.18$ μm attains a maximum speed of $\omega_R/2\pi = 15.1$ GHz with rotational Q-factor of 3.3×10^{14}. In cryogenic environments the pressure is typically of the order of $p \sim 10^{-7}$ mbar. For such low pressures the steady state speed would be larger by 3 orders of magnitude. However, the time the particle takes to reach the steady state is dictated by the gas damping rate, and will take longer. Such high speed will be limited by the elastic tensile where the centrifugal force is strong enough to break the material.

Conclusions.—We have described a magnonic version of the EdH effect, and investigated the interplay between the magnonic OAM and the mechanical rotation. Coherent driving of OAM magnon provides precise control on the mechanical rotation. Our results can be exploited for a variety of purposes such as precision inertial/gyroscopic sensors; preparing and observing coherent superpositions of quantized rotational states; or for future magnonic-hybrid based quantum communication, computing, and memories.

*KaniMohamed@oist.jp

[1] O. W. Richardson, A mechanical effect accompanying magnetization, Phys. Rev. (Series I) **26**, 248 (1908).

[2] A. Einstein and W. J. De Haas, Experimental proof of the existence of Ampére's molecular currents, Proc. KNAW **181**, 696 (1915).

[3] M. Ganzhorn, S. Klyatskaya, M. Ruben, and W. Wernsdorfer, Quantum Einstein-de Haas effect, Nat. Commun. **7**, 11443 (2016).

[4] C. Dornes *et al.*, The ultrafast Einstein-de Haas effect, Nature (London) **565**, 209 (2019).

[5] S. J. Barnett, Magnetization by rotation, Phys. Rev. **6**, 239 (1915).

[6] S. J. Barnett, The magnetization of iron, nickel, and cobalt by rotation and the nature of the magnetic molecule, Phys. Rev. **10**, 7 (1917).

[7] S. J. Barnett, Gyromagnetic and electron-inertia effects, Rev. Mod. Phys. **7**, 129 (1935).

[8] A. Prabhakar and D. D. Stancil, *Spin Waves* (Springer US, Boston, MA, 2009).

[9] J. Harris, V. Grillo, E. Mafakheri, G. C. Gazzadi, S. Frabboni, R. W. Boyd, and E. Karimi, Structured quantum waves, Nat. Phys. **11**, 629 (2015).

[10] M. Uchida and A. Tonomura, Generation of electron beams carrying orbital angular momentum, Nature (London) **464**, 737 (2010).

[11] C. W. Clark, R. Barankov, M. G. Huber, M. Arif, D. G. Cory, and D. A. Pushin, Controlling neutron orbital angular momentum, Nature (London) **525**, 504 (2015).

[12] L. Allen, M. W. Beijersbergen, R. J. C. Spreeuw, and J. P. Woerdman, Orbital angular momentum of light and the transformation of Laguerre-Gaussian laser modes, Phys. Rev. A **45**, 8185 (1992).

[13] R. Marchiano and J.-L. Thomas, Synthesis and analysis of linear and nonlinear acoustical vortices, Phys. Rev. E **71**, 066616 (2005).

[14] R. R. Neumann, A. Mook, J. Henk, and I. Mertig, Orbital Magnetic Moment of Magnons, Phys. Rev. Lett. **125**, 117209 (2020).

[15] Y. Jiang, H. Y. Yuan, Z.-X. Li, Z. Wang, H. W. Zhang, Y. Cao, and P. Yan, Twisted Magnon as a Magnetic Tweezer, Phys. Rev. Lett. **124**, 217204 (2020).

[16] C. Jia, D. Ma, A. F. Schäffer, and J. Berakdar, Twisting and tweezing the spin wave: On vortices, skyrmions, helical waves, and the magnonic spiral phase plate, J. Opt. **21**, 124001 (2019).

[17] C. Jia, M. Chen, A. F. Schäffer, and J. Berakdar, Chiral logic computing with twisted antiferromagnetic magnon modes, npj Comput. Mater. **7**, 101 (2021).

[18] L. R. Walker, Magnetostatic modes in ferromagnetic resonance, Phys. Rev. **105**, 390 (1957).

[19] P. C. Fletcher and R. O. Bell, Ferrimagnetic resonance modes in spheres, J. Appl. Phys. **30**, 687 (1959).

[20] D. Lachance-Quirion, Y. Tabuchi, S. Ishino, A. Noguchi, T. Ishikawa, R. Yamazaki, and Y. Nakamura, Resolving quanta of collective spin excitations in a millimeter-sized ferromagnet, Sci. Adv. **3**, e1603150 (2017).

[21] C. A. Potts, E. Varga, V. A. S. V. Bittencourt, S. V. Kusminskiy, and J. P. Davis, Dynamical Backaction Magnomechanics, Phys. Rev. X **11**, 031053 (2021).

[22] A. Kani, B. Sarma, and J. Twamley, Intensive Cavity-Magnomechanical Cooling of a Levitated Macromagnet, Phys. Rev. Lett. **128**, 013602 (2022).

[23] A. Osada, A. Gloppe, Y. Nakamura, and K. Usami, Orbital angular momentum conservation in Brillouin light scattering within a ferromagnetic sphere, New J. Phys. **20**, 103018 (2018).

[24] A. Leo, A. G. Monteduro, S. Rizzato, L. Martina, and G. Maruccio, Identification and time-resolved study of ferrimagnetic spin-wave modes in a microwave cavity in the strong-coupling regime, Phys. Rev. B **101**, 014439 (2020).

[25] A. Manjavacas and F. J. García de Abajo, Vacuum Friction in Rotating Particles, Phys. Rev. Lett. **105**, 113601 (2010).

[26] Q. Zhu, N. Li, H. Su, W. Li, and H. Hu, A review of optically induced rotation, Front. Inf. Technol. Electron. Eng. **23**, 171 (2022).

[27] R. Reimann, M. Doderer, E. Hebestreit, R. Diehl, M. Frimmer, D. Windey, F. Tebbenjohanns, and L. Novotny, GHz Rotation of an Optically Trapped Nanoparticle in Vacuum, Phys. Rev. Lett. **121**, 033602 (2018).

[28] F. Monteiro, S. Ghosh, E. C. van Assendelft, and D. C. Moore, Optical rotation of levitated spheres in high vacuum, Phys. Rev. A **97**, 051802(R) (2018).

[29] Y. Jin, J. Yan, S. J. Rahman, J. Li, X. Yu, and J. Zhang, 6 GHz hyperfast rotation of an optically levitated nanoparticle in vacuum, Photonics Res. **9**, 1344 (2021).

[30] A. Anhäuser, R. Wunenburger, and E. Brasselet, Acoustic Rotational Manipulation Using Orbital Angular Momentum Transfer, Phys. Rev. Lett. **109**, 034301 (2012).

[31] A. D. Rider, C. P. Blakemore, A. Kawasaki, N. Priel, S. Roy, and G. Gratta, Electrically driven, optically levitated microscopic rotors, Phys. Rev. A **99**, 041802(R) (2019).

[32] M. Schuck, D. Steinert, T. Nussbaumer, and J. W. Kolar, Ultrafast rotation of magnetically levitated macroscopic steel spheres, Sci. Adv. **4**, e1701519 (2018).

[33] J. Ahn, Z. Xu, J. Bang, Y.-H. Deng, T. M. Hoang, Q. Han, R.-M. Ma, and T. Li, Optically Levitated Nanodumbbell

[34] M. Xu, K. Yamamoto, J. Puebla, K. Baumgaertl, B. Rana, K. Miura, H. Takahashi, D. Grundler, S. Maekawa, and Y. Otani, Nonreciprocal surface acoustic wave propagation via magneto-rotation coupling, Sci. Adv. **6**, eabb1724 (2020).

[35] S. P. Wolski, D. Lachance-Quirion, Y. Tabuchi, S. Kono, A. Noguchi, K. Usami, and Y. Nakamura, Dissipation-Based Quantum Sensing of Magnons with a Superconducting Qubit, Phys. Rev. Lett. **125**, 117701 (2020).

[36] D. Lachance-Quirion, Y. Tabuchi, A. Gloppe, K. Usami, and Y. Nakamura, Hybrid quantum systems based on magnonics, Appl. Phys. Express **12**, 070101 (2019).

[37] N. Crescini, C. Braggio, G. Carugno, R. Di Vora, A. Ortolan, and G. Ruoso, Magnon-driven dynamics of a hybrid system excited with ultrafast optical pulses, Commun. Phys. **3**, 164 (2020).

[38] S. Bretzel, G. E. W. Bauer, Y. Tserkovnyak, and A. Brataas, Barnett effect in thin magnetic films and nanostructures, Appl. Phys. Lett. **95**, 122504 (2009).

[39] Y. Acremann, C. H. Back, M. Buess, O. Portmann, A. Vaterlaus, D. Pescia, and H. Melchior, Imaging precessional motion of the magnetization vector, Science **290**, 492 (2000).

[40] C. Gonzalez-Ballestero, D. Hümmer, J. Gieseler, and O. Romero-Isart, Theory of quantum acoustomagnonics and acoustomechanics with a micromagnet, Phys. Rev. B **101**, 125404 (2020).

[41] P. Fletcher, I. H. Solt, and R. Bell, Identification of the magnetostatic modes of ferrimagnetic resonant spheres, Phys. Rev. **114**, 739 (1959).

[42] J. Cho, S. Miwa, K. Yakushiji, S. Tamaru, H. Kubota, A. Fukushima, S. Fujimoto, E. Tamura, C.-Y. You, S. Yuasa, and Y. Suzuki, Spin-wave eigenmodes in single disk-shaped FeB nanomagnet, Phys. Rev. B **94**, 184411 (2016).

[43] M. Chen, A. F. Schäffer, J. Berakdar, and C. Jia, Generation, electric detection, and orbital-angular momentum tunneling of twisted magnons, Appl. Phys. Lett. **116**, 172403 (2020).

[44] L. Vaidman, Torque and force on a magnetic dipole, Am. J. Phys. **58**, 978 (1990).

[45] M. Mansuripur, Trouble with the Lorentz Law of Force: Incompatibility with Special Relativity and Momentum Conservation, Phys. Rev. Lett. **108**, 193901 (2012).

[46] S. Kuhr, S. Gleyzes, C. Guerlin, J. Bernu, U. B. Hoff, S. Deléglise, S. Osnaghi, M. Brune, J.-M. Raimond, S. Haroche, E. Jacques, P. Bosland, and B. Visentin, Ultrahigh finesse Fabry-Pérot superconducting resonator, Appl. Phys. Lett. **90**, 164101 (2007).

[47] C. C. Rusconi and O. Romero-Isart, Magnetic rigid rotor in the quantum regime: Theoretical toolbox, Phys. Rev. B **93**, 054427 (2016).

[48] C. C. Rusconi, V. Pöchhacker, K. Kustura, J. I. Cirac, and O. Romero-Isart, Quantum Spin Stabilized Magnetic Levitation, Phys. Rev. Lett. **119**, 167202 (2017).

[49] Y. B. Band, Y. Avishai, and A. Shnirman, Dynamics of a Magnetic Needle Magnetometer: Sensitivity to Landau-Lifshitz-Gilbert Damping, Phys. Rev. Lett. **121**, 160801 (2018).

[50] I. H. Solt and P. C. Fletcher, Magnetic anisotropy from the magnetostatic modes, J. Appl. Phys. **31**, S100 (1960).

[51] R. G. E. Morris, A. F. van Loo, S. Kosen, and A. D. Karenowska, Strong coupling of magnons in a YIG sphere to photons in a planar superconducting resonator in the quantum limit, Sci. Rep. **7**, 11511 (2017).

[52] M. Matsuo, E. Saitoh, and S. Maekawa, Spin-Mechatronics, J. Phys. Soc. Jpn. **86**, 011011 (2017).

[53] H. Chudo, M. Matsuo, S. Maekawa, and E. Saitoh, Barnett field, rotational Doppler effect, and Berry phase studied by nuclear quadrupole resonance with rotation, Phys. Rev. B **103**, 174308 (2021).

[54] M. Arabgol and T. Sleator, Observation of the Nuclear Barnett Effect, Phys. Rev. Lett. **122**, 177202 (2019).

[55] A. Gloppe, R. Hisatomi, Y. Nakata, Y. Nakamura, and K. Usami, Resonant Magnetic Induction Tomography of a Magnetized Sphere, Phys. Rev. Appl. **12**, 014061 (2019).

[56] A. Romanenko, R. Pilipenko, S. Zorzetti, D. Frolov, M. Awida, S. Belomestnykh, S. Posen, and A. Grassellino, Three-dimensional superconducting resonators at $T <$ 20 mK with photon lifetimes up to $\tau = 2$ s, Phys. Rev. Appl. **13**, 034032 (2020).